Metals **2014**, *4*, 388-400; doi:10.3390/met4030388

OPEN ACCESS

metals

ISSN 2075-4701

www.mdpi.com/journal/metals/

Article

Investigation of Effect of Milling Atmosphere and Starting Composition on Mg_2FeH_6 Formation

Alexandre Augusto Cesario Asselli and Jacques Huot *

Hydrogen Research Institute, Université du Québec à Trois-Rivières, 3351, boul. des Forges, C.P. 50, Trois-Rivières (Québec) G9A 5H7, Canada; E-Mail: asselli@gmail.com

* Author to whom correspondence should be addressed; E-Mail: Jacques.huot@uqtr.ca; Tel.: +1-819-376-5011 (ext. 3576); Fax: +1-819-376-5164.

Received: 17 July 2014; in revised form: 1 August 2014 / Accepted: 8 August 2014 / Published: 14 August 2014

Abstract: In this study we investigated the synthesis and the hydrogen storage properties of Mg_2FeH_6. The complex hydride was prepared by ball milling under argon and hydrogen atmosphere from 2Mg + Fe and $2MgH_2$ + Fe compositions. The samples were characterized by X-ray powder diffraction and scanning electron microcopy. Kinetics of hydrogen absorption and desorption were measured in a Sievert's apparatus. We found that the milling atmosphere plays a more important role on Mg_2FeH_6 synthesis than the starting compositions. Ball milling under hydrogen pressure resulted in smaller particles sizes and doubled the yield of Mg_2FeH_6 formation. Despite the microstructural differences after ball milling, all samples had similar hydrogen absorption and desorption kinetics. Loss of capacity was observed after only five cycles of hydrogen absorption/desorption.

Keywords: metal hydride; Mg_2FeH_6; ball milling; hydrogen storage

1. Introduction

The complex hydride Mg_2FeH_6 has the highest known volumetric density of hydrogen (150 kg m^{-3}), which is more than twice higher than hydrogen in liquid state (70.8 kg m^{-3}) [1]. This high hydrogen density is attractive for solid-state hydrogen storage applications. However, the high operating temperature, owing to the thermodynamic stability of the hydride, limits its use for stationary applications. On the other hand, the important enthalpy of hydride formation makes this material

interesting for thermochemical thermal energy storage [2]. However, the synthesis of Mg_2FeH_6 as a pure material is a great challenge, mainly due to the immiscibility of magnesium and iron [3].

In 1984, Didisheim *et al.* [4] reported the first synthesis of Mg_2FeH_6 by sintering the metallic elements at high temperature (450–520 °C) under hydrogen pressure (20–120 bar) during several days (2–10 days). Despite the severe sintering conditions, the yield of Mg_2FeH_6 was only 50%. Later, Selvan and Yvon [5] showed that the most convenient condition to synthesize the Mg_2FeH_6 was by sintering of 2Mg + Fe at 450 °C under 90 bar of H_2 pressure during 10 days. Huot *et al.* [6] demonstrated that Mg_2FeH_6 could be synthesize in mild condition (350 °C, 50 bar of H_2, 24 h) by ball milling of 2Mg + Fe under argon or hydrogen atmosphere for 20 h before sintering. Furthermore, the synthesis of Mg_2FeH_6 at room temperature was reported by high energy ball milling of $2MgH_2$ + Fe under argon atmosphere [7] and by reactive milling of the metallic elements under hydrogen pressure [8].

The synthesis of Mg_2FeH_6 by ball milling has been studied by several authors using different milling parameters, such as: type of mill; ball to powder ratio; number and size of balls; milling time; rotational speed; milling atmosphere and hydrogen pressure [9–23]. Irrespective of the milling conditions, some iron was always detected in the milled powder representing an incomplete Mg_2FeH_6 formation. Regardless of all these results concerning the Mg_2FeH_6 synthesis, the effect of milling parameters on the kinetics of hydrogen absorption/desorption has not been thoroughly investigated.

Besides the synthesis, the mechanism of Mg_2FeH_6 formation has been discussed in several papers. Some authors reported that Mg_2FeH_6 is formed from the metallic elements [2,4,19,24], while others claimed that MgH_2 is the Mg_2FeH_6 precursor [9,20,21,25,26]. Recently, we studied the transformation of phases during hydrogen absorption of a ball milled 2Mg + Fe mixture [27]. We showed that MgH_2 is formed with very fast kinetics, and then, in a much slower reaction, MgH_2 reacts with Fe to form Mg_2FeH_6. Danaie *et al.* [28] observed this transformation of phases by TEM and found that Mg_2FeH_6 nucleates between MgH_2 and Fe particles, and then, grows with a columnar morphology. Although these results confirm the formation of Mg_2FeH_6 from MgH_2, the direct reaction from the metallic elements is also feasible. As Mg_2FeH_6 is thermodynamically more stable than MgH_2, the direct reaction can take place under specific conditions of temperature and hydrogen pressure.

In this study, we investigated the effects of milling atmosphere and starting compositions on the microstructure, Mg_2FeH_6 formation and hydrogen storage properties of ball milled materials. The Mg_2FeH_6 was synthesized from 2Mg + Fe and $2MgH_2$ + Fe compositions by ball milling under argon and hydrogen atmosphere. Short cycles of hydrogen absorption/desorption were performed to evaluate the influence of ball milling on the kinetics and hydrogen storage capacity. The reaction pathway of Mg_2FeH_6 formation is also discussed.

2. Materials and Methods

Two compositions, $2MgH_2$ + Fe and 2Mg + Fe, were prepared from magnesium hydride (mesh 300, 98%), magnesium (–325 mesh, 99.8%) and iron (–22 mesh, 98%) powders, all provided by Alfa Aesar. The mixtures weighting about 2 grams were loaded together with 20 balls (10 mm in diameter) into a high pressure milling vial of internal volume of 218 cm^3. Both balls and vial were made of hardened

stainless steel. The ball-to-powder weight ratio was 40:1. All handlings were performed inside an argon filled glovebox.

Ball milling was carried out in a Fritsch's vario-planetary mill pulverisette 4. The relative speed ratio between the milling vial and the main disk was set to −1.82, the minus sign meaning that the vial's direction of rotation was opposite to the main disk rotation direction. The samples were milled at 330 rpm (main disk speed) for 12 h. The $2MgH_2$ + Fe composition was ball milled under argon atmosphere and 3 MPa of hydrogen pressure. The 2Mg + Fe sample was only ball milled under 3 MPa of H_2. These samples are respectively named $2MgH_2$ + Fe (Ar), $2MgH_2$ + Fe (H_2) and 2Mg + Fe (H_2).

The crystal structure of the ball milled materials was investigated by X-ray powder diffraction (XRPD). For XRPD measurements, a small amount of the ball milled samples was mounted on a sealed flat plate sample holder inside the glovebox. This procedure was used in order to never expose the sample to air. The samples were analyzed on a Bruker's D8 Focus diffractometer with a Bragg-Brentano configuration using CuKα radiation. The percentage of phases as well as the average crystallite size were evaluated from the XRPD patterns by Rietveld method using GSAS [29] and EXPGUI [30] softwares. Morphology of ball milled powders was characterized by scanning electron microscopy (SEM) using a Tescan Vega3-SB microscope (ICMCB, Bordeaux, France).

The concentration of Fe in the ball milled powders was measured by atomic absorption spectrometry (AAS) to evaluate a possible Fe contamination from the balls and vial by milling. Samples of approximately 100 mg were dissolved in a 100 mL mixture of HCl (10% in volume) and distilled water, and analyzed in a Varian's SpectrAA 50/55 spectrometer.

Kinetic curves of hydrogen absorption/desorption were measured using a homemade Sieverts' apparatus. Samples of around 100 mg were loaded and sealed into the sample holder inside the glovebox. The first hydrogen desorption was studied under 100 kPa of H_2 during heating at 10 °C min^{-1} from room temperature up to 400 °C. After completed hydrogen desorption, 5 cycles of hydrogen absorption/desorption were measured at 400 °C. The kinetics of hydrogen absorption was measured for 1 hour under initial H_2 pressure of 2.5 and 1.7 MPa. In the case of hydrogen desorption, the H_2 pressure of the system was set to 100 kPa.

To investigate the transformation of phases upon hydrogenation, samples were "quenched" during the kinetic experiments under H_2 pressure. "Quenching" was achieved by closing the sample valve and cooling the sample holder down to room temperature in a few seconds using a water bath. As MgH_2 and Mg_2FeH_6 are both highly stable hydrides, the changes of phase composition and hydrogen capacity are minimal after quenching. Thus, the XRPD patterns of quenched samples truly reflect the phases present during the reaction of hydrogen absorption.

3. Results and Discussion

3.1. Ball Milling

The XRPD patterns of the ball milled samples are shown in Figure 1. The presence of a high background at low angles in all XRPD patterns is due to the protective dome of the sealed sample holder. The use of this protective dome was required to prevent air exposure and formation of MgO phase [31]. The XRPD patterns show that Mg_2FeH_6 was synthesized by ball milling regardless of

starting compositions and milling atmospheres. However, diffraction peaks of α-Fe phase were identified in all samples. This means an incomplete formation of Mg_2FeH_6 despite the long milling time. In the case of the $2MgH_2$ + Fe composition processed under argon atmosphere, the presence of iron after ball milling was expected due to stoichiometry of the reactants and milling atmosphere. The XRPD pattern of this sample also presented small diffraction peaks corresponding to β-MgH_2 and Mg phases. For the $2MgH_2$ + Fe and 2Mg + Fe samples ball milled under H_2 pressure, only Mg_2FeH_6 and α-Fe phases were clearly identified. As some free Fe was still present after milling, it means that one would expect to identify Mg and/or β-MgH_2 phases in these two samples. However, it should be taken into account that the detection of these phases can be quite difficult due to their smaller number of electrons and volume fraction in comparison to Mg_2FeH_6 and α-Fe. Another explanation could be an iron contamination from the balls and vial by milling. To assess this possible contamination, we measured the Fe concentration on the ball milled samples by atomic absorption spectrometry (AAS). Table 1 presents the results of AAS of the ball milled samples**.** For comparison, the nominal compositions of Fe before ball milling are also indicated. The results showed that the Fe concentrations on the processed samples were similar to nominal values. Therefore, ball milling did not modify the iron composition of the samples.

Figure 1. XRPD patterns of ball milled samples. The position of X-ray diffraction peaks for the identified phases are indicated below the patterns.

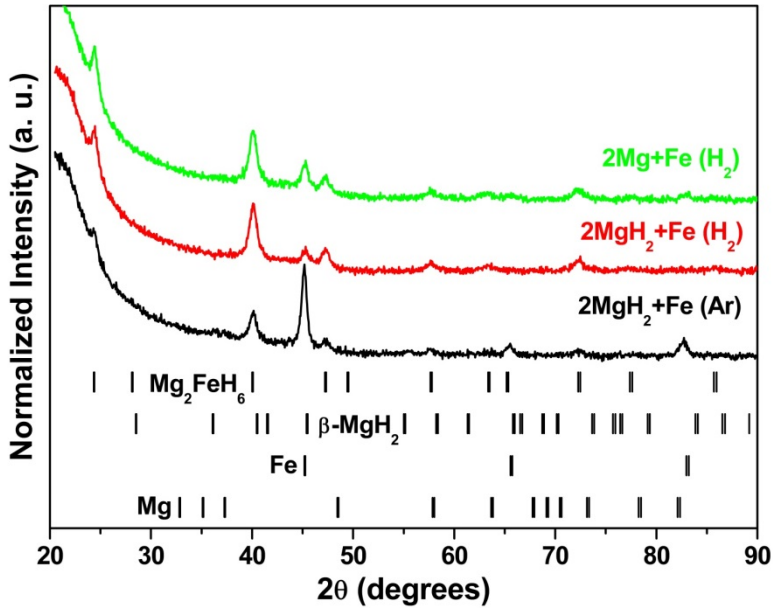

Table 1. Iron concentration (wt. %) of ball milled samples measured by atomic absorption spectrometry. The nominal composition before ball milling is also presented for comparison.

	$2MgH_2$ + Fe (Ar)	**$2MgH_2$ + Fe (H_2)**	**2Mg + Fe (H_2)**
Nominal composition	51.48	51.48	53.45
After ball milling	54.63	51.59	51.14

Rietveld refinement was performed on the XRPD patterns to get a quantitative analysis and evaluate the effects of starting composition and milling atmosphere on the Mg_2FeH_6 formation. Table 2 summarizes the phase abundance in wt. % as well as the average crystallite size calculated from the Rietveld refinement. As expected, ball milling $2MgH_2$ + Fe under argon atmosphere produced the lowest yield of Mg_2FeH_6 (about 41 wt. %). Ball milling under H_2 pressure doubled the amount of Mg_2FeH_6 phase. The average crystallite size estimated for all phases were of the same order of magnitude (10 to 20 nm).

Table 2. Relative quantities and crystallite size of phases identified in the ball milled samples as calculated by Rietveld refinement. In parenthesis are uncertainties on the last significant digit.

Phase		$2MgH_2$ + Fe (Ar)	$2MgH_2$ + Fe (H_2)	2Mg + Fe (H_2)
Mg_2FeH_6	wt. %	41.4 (6)	88.2 (1)	81.7 (2)
	size (nm)	12	11	16
α-Fe	wt. %	47.6 (4)	11.8 (5)	18.3 (6)
	size (nm)	16	14	12
β-MgH_2	wt. %	6.6 (9)	-	-
	size (nm)	21	-	-
Mg	wt. %	4.4 (9)	-	-
	size (nm)	21	-	-

3.2. Microstructural Characterization

The microstructure of the ball milled materials was investigated by scanning electron microscopy (SEM). Figure 2 shows the SEM micrographs using a secondary electron (SE) and back-scattered electron (BSE) detectors. From the SE micrographs, the difference in particle size between the samples processed under H_2 pressure and Ar atmosphere is evident. The particle sizes of the $2MgH_2$ + Fe (Ar) sample were in the range of 3 to 10 μm. For the samples prepared under H_2 pressure, the particle sizes were smaller than 3 μm. It shows that milling atmosphere plays a more important role on the final particle size than the nature of the starting composition. Furthermore, the BSE micrographs of the sample milled in Ar presented brighter spots of 30–40 nm distributed over the larger particles. These spots correspond to Fe-rich regions. This feature was barely seen for the others samples. Thus, ball milling under H_2 also results in better homogeneity and microstructure refinement.

Our results are different from the study of Castro and Gennari [11]. These authors investigated the synthesis of Mg_2FeH_6 by ball milling under H_2 pressure. They showed that the synthesis time of Mg_2FeH_6 from a $2MgH_2$ + Fe composition was almost twice longer and yielded practically half of Mg_2FeH_6 than when a 2Mg + Fe composition was milled at the same experimental condition. The authors attributed the results to the unlike mechanical properties and microstructures of the starting compositions. It should be pointed out that they synthesized less than 30 wt. % of Mg_2FeH_6 by ball milling 2Mg + Fe for 60 h. In the case of the $2MgH_2$ + Fe composition, the maximum yield of Mg_2FeH_6 was only 15.6 wt. % after 100 h of ball milling. In our case, the microstructure and the synthesis of Mg_2FeH_6 were mostly affected by the milling atmosphere than the nature of starting composition. A possible explanation of the discrepancies between their results and ours could be the

milling parameters. They used a less energetic milling device (Uni-ball-Mill II) and lower hydrogen pressure (0.5 MPa), which could have hindered the Mg_2FeH_6 formation.

Figure 2. SEM micrographs of ball milled samples. The **left** and **right** columns show respectively the secondary (SE) and back-scattered electron (BSE) micrographs.

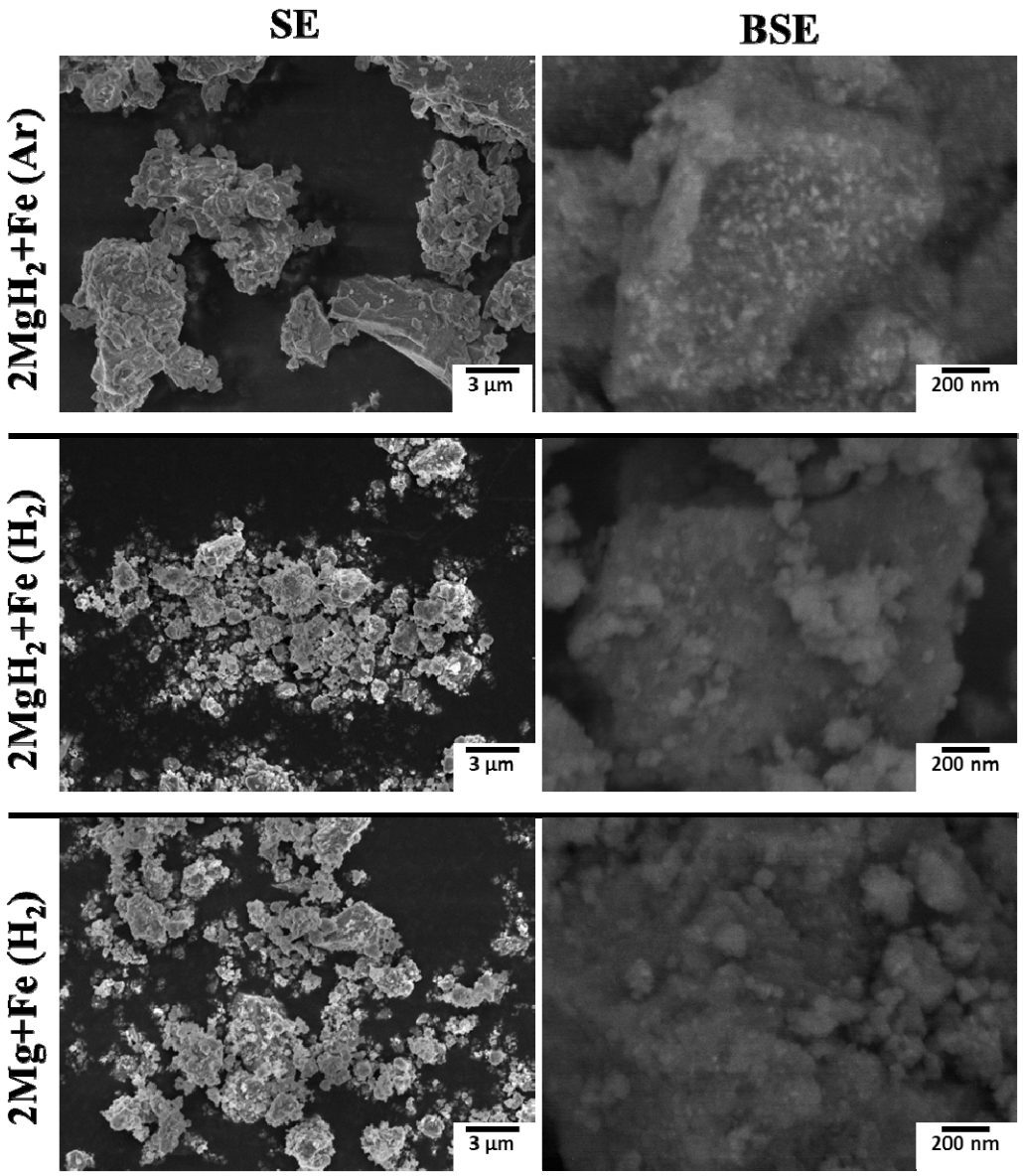

3.3. Hydrogen Desorption under Heating

After ball milling, the first hydrogen desorption was studied by heating the samples under 100 kPa of H_2 from room temperature up to 400 °C at 10 °C min^{-1}. Figure 3 presents the simultaneous curves of hydrogen capacity and temperature ramp of the ball milled powders. The samples showed a similar desorption behavior but with different amounts of hydrogen released. The $2MgH_2$ + Fe composition ball milled under argon atmosphere had the lowest hydrogen gravimetric capacity (3.59 wt. %). This value is very close to the theoretical hydrogen capacity of the starting composition (3.62 wt. %). However, this material absorbed 0.32 wt. % of hydrogen from 130 up to 245 °C. As shown in Figure 1, Mg diffraction peaks were identified on the XRPD pattern of this sample. Thus, considering the

hydrogen capacity of MgH_2 (7.6 wt. %), one can calculate that a hydrogen absorption of 0.32 wt. % requires 3.89 wt. % of magnesium. This percentage of Mg is close to the relative quantity estimated by Reitveld refinement in Table 2 (4.4 wt. %). Therefore, this hydrogen absorption occurring at around 150 °C could be attributed to the formation of β-MgH_2 from magnesium.

Figure 3. Curves of hydrogen desorption under 100 kPa of H_2 during heating at 10 °C min^{-1}.

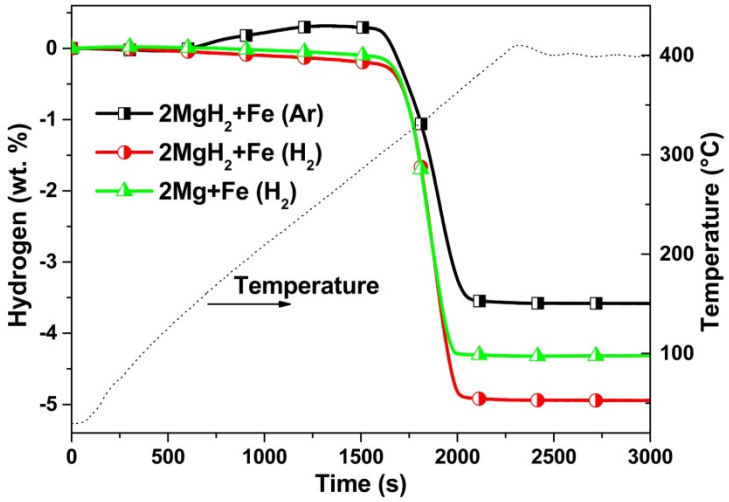

As expected, ball milling the $2MgH_2$ + Fe and 2Mg + Fe compositions under hydrogen atmosphere led to higher capacities of 4.94 and 4.32 wt. %, respectively. Assuming that Mg_2FeH_6 is the only hydride phase present on these samples, as suggested by the XRPD results, one can determine the percentage of Mg_2FeH_6 from the hydrogen capacity. Dividing the capacity of hydrogen desorption by the theoretical hydrogen capacity of Mg_2FeH_6 (5.4 wt. %), we find that the percentage of Mg_2FeH_6 phase on the $2MgH_2$ + Fe (H_2) and 2Mg + Fe (H_2) samples are respectively 91.5 wt.% and 80 wt. %. These values are in agreement with the results of Rietveld refinement. The difference in hydrogen capacity between these two samples could be explained by the reaction pathway of Mg_2FeH_6 formation. During ball milling of the metallic elements (2Mg + Fe) under H_2 pressure, the β-MgH_2 phase is firstly formed and then, it reacts with Fe to form the complex hydride Mg_2FeH_6 [22]. Using instead MgH_2 as starting material is a shortcut to Mg_2FeH_6 formation and result in higher hydrogen capacity.

3.4. Kinetics of Hydrogen Absorption and Desorption

After complete hydrogen desorption, five cycles of hydrogen absorption and desorption were performed at 400 °C. The initial H_2 pressure was set to 2.5 MPa for absorption and 100 kPa for desorption. The kinetic curves of hydrogen absorption and desorption are presented in Figure 4. The "Reacted fraction" *y*-axis represents the ratio of measured hydrogen capacity to the maximum theoretical capacity of the samples (5.4 wt. %). Despite having different particle sizes and phase compositions after ball milling, all samples presented similar kinetics of hydrogen absorption and desorption. Hydrogen absorption was practically completed in less than five minutes but the samples did not absorb more than 75% of the theoretical hydrogen capacity. Moreover, from cycle 1 to 3,

we observed for all samples a decrease in hydrogen capacity. From third to fifth cycle, the hydrogen capacities were practically constant. In the last cycle, the hydrogen capacity of the $2MgH_2$ + Fe (Ar) sample was around 60% of the theoretical capacity. For the 2Mg + Fe (H_2) and $2MgH_2$ + Fe (H_2) samples, the hydrogen absorption respectively stabilized around 65 and 68% of the maximum capacity. In the case of hydrogen desorption, similar kinetics was observed for all samples.

Figure 4. Kinetic curves of hydrogen absorption and desorption at 400 °C of ball milled samples: (**a**) and (**b**) $2MgH_2$ + Fe (Ar); (**c**) and (**d**) $2MgH_2$ + Fe (H_2) and (**e**) and (**f**) 2Mg + Fe (H_2). The hydrogen absorption and desorption were respectively measured under 2.5 MPa and 100 kPa of H_2.

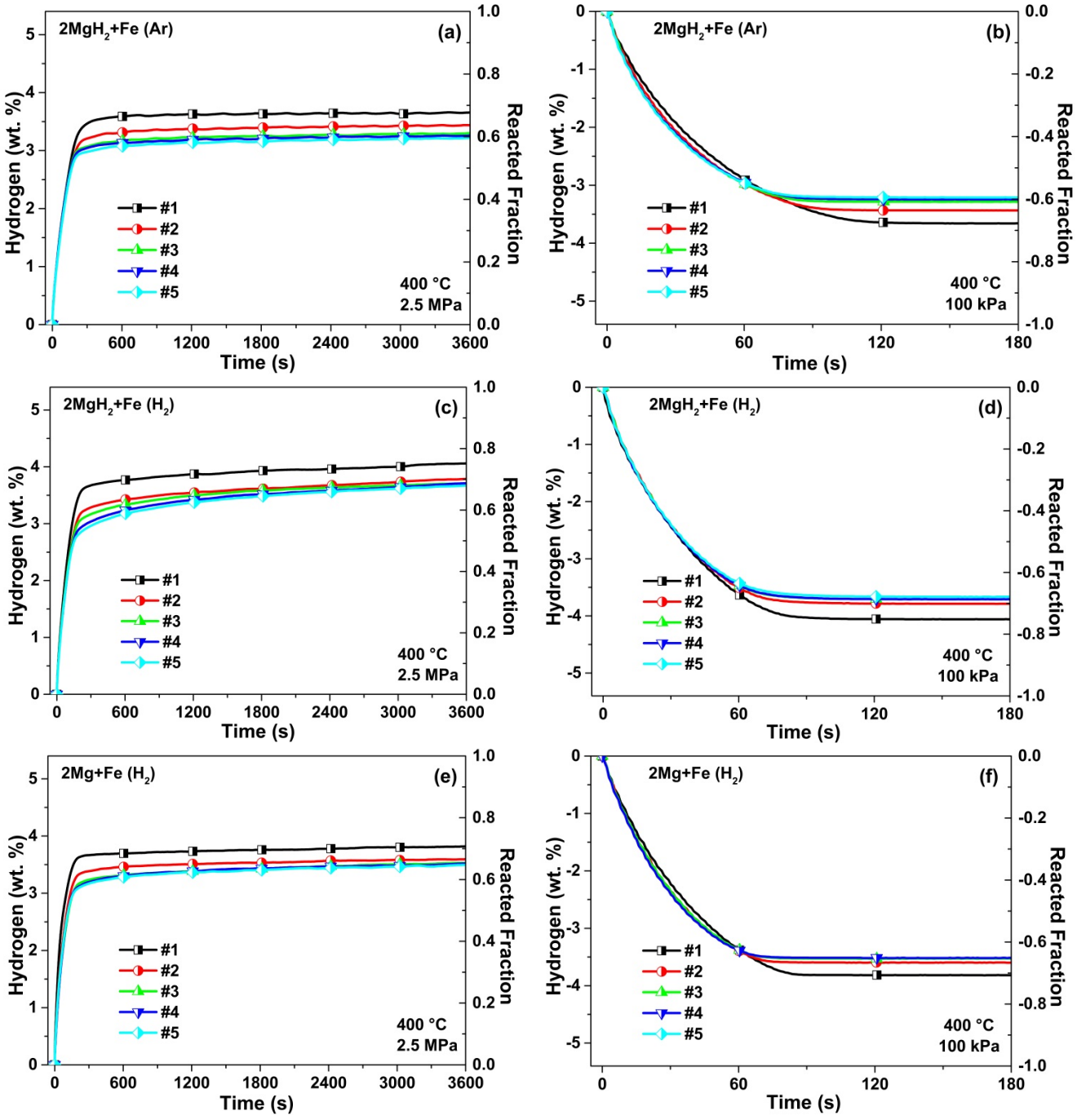

According to the study of Bogdanović *et al*. [2], the equilibrium pressure at 400 °C of Mg_2FeH_6 and MgH_2 are 1.12 and 1.97 MPa, respectively. Therefore, the formation of both β-MgH_2 and Mg_2FeH_6 phases are thermodynamically favorable at 400 °C under 2.5 MPa of H_2. We recently showed that under conditions where the formation of both hydrides are thermodynamically possible, Mg_2FeH_6 is preferentially formed from a two-step reaction where β-MgH_2 plays the role of Mg_2FeH_6 precursor [27,28]. Despite being thermodynamically less stable than Mg_2FeH_6, β-MgH_2 is firstly formed due to its faster kinetics of formation [27]. Afterward, Mg_2FeH_6 nucleates between β-MgH_2 and α-Fe phases, and grows with a columnar morphology in a slow diffusional process [28]. Consequently, the kinetics of this diffusional reaction restrains the formation of Mg_2FeH_6 and result in lower hydrogen storage capacity. However, this is not the only reaction pathway for Mg_2FeH_6 formation. The complex hydride can also be formed directly from the metallic elements. This reaction is possible because MgH_2 has a higher equilibrium pressure than Mg_2FeH_6. Thus, if the H_2 pressure is higher than the equilibrium pressure of Mg_2FeH_6 but lower than MgH_2, the formation of MgH_2 would be thermodynamically restricted and Mg_2FeH_6 would form directly from magnesium and iron.

Figure 5. Kinetic curves of hydrogen absorption at 400 °C before quenching under 1.7 and 2.5 MPa of H_2.

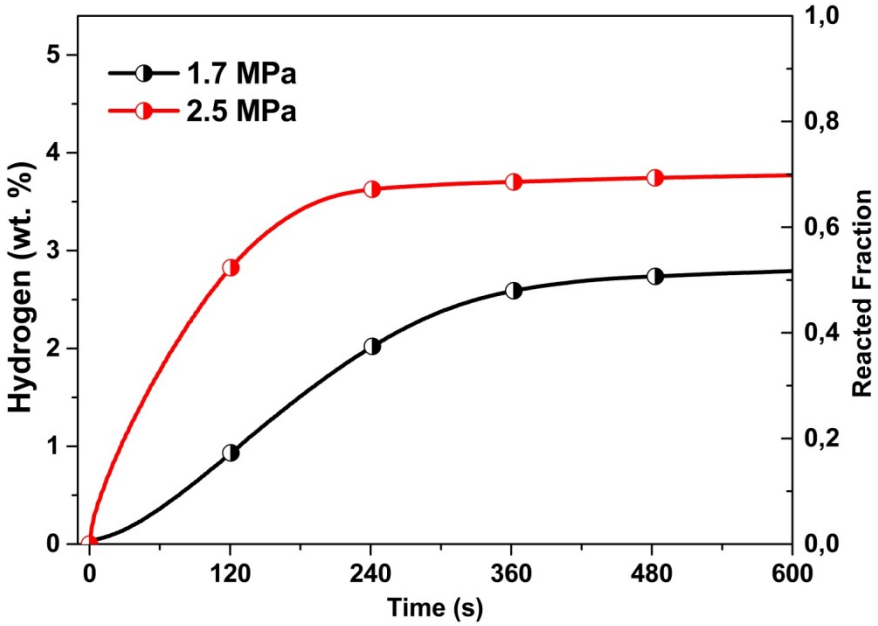

To confirm these two pathways of Mg_2FeH_6 formation, we investigated the transformation of phases upon hydrogenation by quenching two samples under H_2 pressure. For this investigation we used the $2MgH_2$ + Fe (H_2) sample after complete hydrogen desorption. Quenching was carried out after 10 minutes of hydrogen absorption at 400 °C under two hydrogen pressures: 1.7 MPa where only the direct reaction from metallic elements is possible and 2.5 MPa where the two-steps reaction is possible. The kinetic curves of hydrogen absorption before quenching are presented in Figure 5. The hydrogen absorption under 2.5 MPa of H_2 was faster and the hydrogen capacity was 35% higher than when the absorption was performed under 1.7 MPa. This result is attributed to the fast formation of MgH_2, as confirmed by the XRPD patterns shown in Figure 6. In the case of the sample quenched under 1.7 MPa, the XRPD pattern shows the presence of Mg diffraction peaks but, as expected, none

from β-MgH_2 phase. This confirms that under this hydrogenation condition, Mg_2FeH_6 is formed directly from the metallic elements. Results of Rietveld refinement shown in Table 3 indicate that a higher proportion of Mg_2FeH_6 is formed in the direct reaction than in the two-steps reaction. However, hydrogenation under higher H_2 pressure resulted in faster kinetics and higher hydrogen capacity due to the formation of β-MgH_2.

Figure 6. XRPD patterns of quenched samples under 1.7 and 2.5 MPa of H_2.

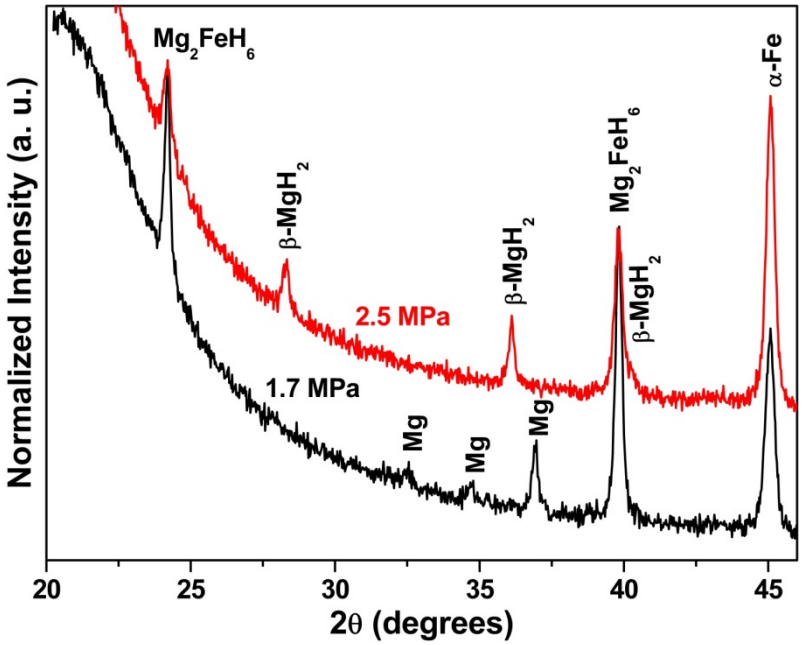

Table 3. Relative quantities and crystallite size of identified phases in the "quenched" samples during hydrogen absorption tests under 1.7 and 2.5 MPa of H_2 as calculated by Rietveld refinement. In parenthesis are uncertainties on the last significant digit.

Phase		1.7 MPa	2.5 MPa
Mg_2FeH_6	wt. %	55.9 (2)	38.6 (3)
	size (nm)	45	29
α-Fe	wt. %	27.8 (2)	37.5 (2)
	size (nm)	30	36
β-MgH_2	wt. %	-	24.0 (5)
	size (nm)	-	42
Mg	wt. %	16.3 (4)	-
	size (nm)	46	-

The effect of cycling under direct reaction condition was studied. Five consecutive cycles of absorption/desorption at 400 °C under respectively 1.7 MPa and 100 kPa were measured and are shown in Figure 7. Despite different pathways of Mg_2FeH_6 formation, the kinetic curves of the direct (Figure 7) and two-step (Figure 3) reactions presented similar loss of hydrogen storage capacity.

Figure 7. Kinetic curves of hydrogen (**a**) absorption and (**b**) desorption at 400 °C of $2MgH_2$ + Fe (H_2) sample. The hydrogen absorption and desorption were respectively measured under 1.7 MPa and 100 kPa of H_2.

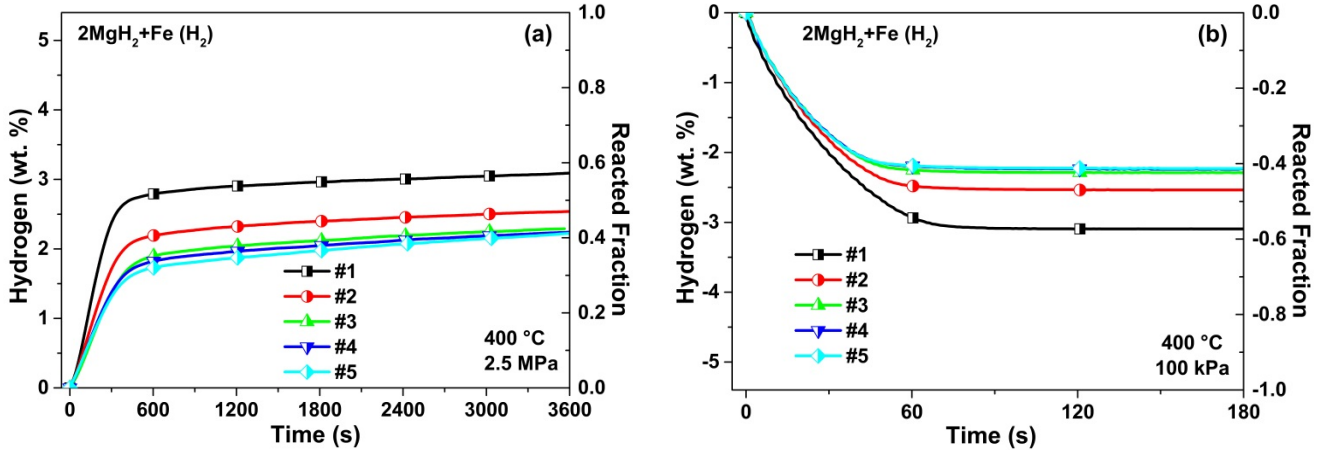

4. Conclusions

We investigated the effect of milling atmosphere and starting compositions on Mg_2FeH_6 formation. Samples of $2MgH_2$ + Fe and 2Mg + Fe compositions were processed by ball milling under argon and hydrogen atmosphere. The milling atmosphere played a more important role on the Mg_2FeH_6 synthesis than the nature of the starting compositions. Ball milling under hydrogen resulted in smaller particle sizes, better homogeneity and microstructure refinement, and moreover, doubled the yield of Mg_2FeH_6 formation. Despite having different particle sizes and phase compositions after ball milling, all samples presented similar kinetics of hydrogen desorption. The transformation of phases upon hydrogenation was investigated by quenching samples under H_2 pressure. Depending on the hydrogenation conditions (temperature and H_2 pressure), the complex hydride can be formed from two reaction pathways: (1) directly from the metallic elements; or (2) in a two-step reaction where MgH_2 plays the role of Mg_2FeH_6 precursor. Regardless of reaction pathway, loss of hydrogen capacity was measured after only five cycles of hydrogen absorption/desorption.

Acknowledgments

The authors would like to thank J.L. Bobet for electron microscopy and F. Lafontaine for atomic absorption measurements. A.A.C.A. is thankful to Fonds de Recherche du Québec–Nature et Technologies for his post-doctoral fellowship. Part of this investigation was supported by funding project C-26/211of the Ministry of Education of Perm Region (Russia). This work was also funded by a discovery grant from Natural Sciences and Engineering Research Council of Canada.

Conflicts of Interest

The authors declare no conflict of interest.

References

1. Züttel, A. Materials for hydrogen storage. *Mater. Today* **2003**, 24–33.
2. Bogdanović, B.; Reiser, A.; Schlichte, K.; Spliethoff, B.; Tesche, B. Thermodynamics and dynamics of the Mg–Fe–H system and its potential for thermochemical thermal energy storage. *J. Alloys Compd.* **2002**, *345*, 77–89.
3. Nayeb-Hashemi, A.A.; Clark, J.B.; Swartzendruber, L.J. The Fe−Mg (Iron-Magnesium) system. *Bull. Alloy Phase Diagrams* **1985**, *6*, 235–238.
4. Didisheim, J.J.; Zolliker, P.; Yvon, K.; Fischer, P.; Schefer, J.; Gubelmann, M.; Williams, A.F. Dimagnesium iron(II) hydride, Mg_2FeH_6, containing octahedral FeH_6^{4-} anions. *Inorg. Chem.* **1984**, *23*, 1953–1957.
5. Selvam, P.; Yvon, K. Synthesis of Mg_2FeH_6, Mg_2CoH_5 and Mg_2NiH_4 by high-pressure sintering of the elements. *Int. J. Hydrogen Energy* **1991**, *16*, 615–617.
6. Huot, J.; Hayakawa, H.; Akiba, E. Preparation of the hydrides Mg_2FeH_6 and Mg_2CoH_5 by mechanical alloying followed by sintering. *J. Alloys Compd.* **1997**, *248*, 164–167.
7. Huot, J.; Boily, S.; Akiba, E.; Schulz, R. Direct synthesis of Mg_2FeH_6 by mechanical alloying. *J. Alloys Compd.* **1998**, *280*, 306–309.
8. Sai Raman, S.S.; Davidson, D.J.; Bobet, J.-L.; Srivastava, O.N. Investigations on the synthesis, structural and microstructural characterizations of Mg-based K_2PtCl_6 type (Mg_2FeH_6) hydrogen storage material prepared by mechanical alloying. *J. Alloys Compd.* **2002**, *333*, 282–290.
9. Gennari, F.; Castro, F.; Andrade Gamboa, J.J. Synthesis of Mg_2FeH_6 by reactive mechanical alloying: formation and decomposition properties. *J. Alloys Compd.* **2002**, *339*, 261–267.
10. Shang, C.X.; Bououdina, M.; Guo, Z.X. Direct mechanical synthesis and characterisation of $Mg_2Fe(Cu)H_6$. *J. Alloys Compd.* **2003**, *356–357*, 626–629.
11. Castro, F.J.; Gennari, F.C. Effect of the nature of the starting materials on the formation of Mg_2FeH_6. *J. Alloys Compd.* **2004**, *375*, 292–296.
12. Herrich, M.; Ismail, N.; Lyubina, J.; Handstein, A.; Pratt, A.; Gutfleisch, O. Synthesis and decomposition of Mg_2FeH_6 prepared by reactive milling. *Mater. Sci. Eng. B* **2004**, *108*, 28–32.
13. Li, S.; Varin, R.A.; Morozova, O.; Khomenko, T. Controlled mechano-chemical synthesis of nanostructured ternary complex hydride Mg2FeH6 under low-energy impact mode with and without pre-milling. *J. Alloys Compd.* **2004**, *384*, 231–248.
14. Varin, R.A.; Li, S.; Calka, A.; Wexler, D. Formation and environmental stability of nanocrystalline and amorphous hydrides in the 2Mg–Fe mixture processed by controlled reactive mechanical alloying (CRMA). *J. Alloys Compd.* **2004**, *373*, 270–286.
15. Varin, R.A.; Li, S.; Chiu, C.; Guo, L.; Morozova, O.; Khomenko, T.; Wronski, Z. Nanocrystalline and non-crystalline hydrides synthesized by controlled reactive mechanical alloying/milling of Mg and Mg–X (X = Fe, Co, Mn, B) systems. *J. Alloys Compd.* **2005**, *404–406*, 494–498.
16. Varin, R.A.; Li, S.; Wronski, Z.; Morozova, O.; Khomenko, T. The effect of sequential and continuous high-energy impact mode on the mechano-chemical synthesis of nanostructured complex hydride Mg_2FeH_6. *J. Alloys Compd.* **2005**, *390*, 282–296.

17. Zhou, D.W.; Li, S.L.; Varin, R.A.; Peng, P.; Liu, J.S.; Yang, F. Mechanical alloying and electronic simulations of 2Mg–Fe mixture powders for hydrogen storage. *Mater. Sci. Eng. A* **2006**, *427*, 306–315.
18. Puszkiel, J.A.; Arneodo Larochette, P.; Gennari, F.C. Hydrogen storage properties of Mg_xFe (x: 2, 3 and 15) compounds produced by reactive ball milling. *J. Power Sources* **2009**, *186*, 185–193.
19. Riktor, M.D.; Deledda, S.; Herrich, M.; Gutfleisch, O.; Fjellvåg, H.; Hauback, B.C. Hydride formation in ball-milled and cryomilled Mg–Fe powder mixtures. *Mater. Sci. Eng. B* **2009**, *158*, 19–25.
20. Leiva, D.R.; de Souza Villela, A.C.; Paiva-Santos, C.D.O.; Fruchart, D.; Miraglia, S.; Ishikawa, T.T.; Botta, W.J. High-Yield Direct Synthesis of Mg_2FeH_6 from the Elements by Reactive Milling. *Solid State Phenom.* **2011**, *170*, 259–262.
21. Asselli, A.A.C.; Leiva, D.R.; Jorge, A.M.; Ishikawa, T.T.; Botta, W.J. Synthesis and hydrogen sorption properties of Mg_2FeH_6–MgH_2 nanocomposite prepared by reactive milling. *J. Alloys Compd.* **2012**, *536*, S250–S254.
22. Asselli, A.A.C.; Jorge, A.M., Jr.; Ishikawa, T.T.; Botta Filho, W.J. Mg_2FeH_6-based nanocomposites with high capacity of hydrogen storage processed by reactive milling. *Mater. Res.* **2012**, *15*, 229–235.
23. Leiva, D.R.; Zepon, G.; Asselli, A.A.C.; Fruchart, D.; Miraglia, S.; Ishikawa, T.T.; Botta, W.J. Mechanochemistry and H-sorption properties of Mg_2FeH_6-based nanocomposites. *Int. J. Mater. Res.* **2012**, *103*, 1147–1154.
24. Puszkiel, J.A.; Larochette, P.A.; Gennari, F.C. Thermodynamic and kinetic studies of Mg–Fe–H after mechanical milling followed by sintering. *J. Alloys Compd.* **2008**, *463*, 134–142.
25. Polanski, M.; Nielsen, T.K.; Cerenius, Y.; Bystrzycki, J.; Jensen, T.R. Synthesis and decomposition mechanisms of Mg_2FeH_6 studied by in-situ synchrotron X-ray diffraction and high-pressure DSC. *Int. J. Hydrogen Energy* **2010**, *35*, 3578–3582.
26. Puszkiel, J.; Gennari, F.; Larochette, P.A.; Karimi, F.; Pistidda, C.; Gosalawit-Utke, R.; Jepsen, J.; Jensen, T.R.; Gundlach, C.; von Colbe, J.B.; Klassen, T.; Dornheim, M. Sorption behavior of the MgH_2–Mg_2FeH_6 hydride storage system synthesized by mechanical milling followed by sintering. *Int. J. Hydrogen Energy* **2013**, *38*, 14618–14630.
27. Asselli, A.A.C.; Botta, W.J.; Huot, J. Formation reaction of Mg_2FeH_6: Effect of hydrogen absorption/desorption kinetics. *Mater. Res.* **2013**, *16*, 1373–1378.
28. Danaie, M.; Asselli, A.A.C.; Huot, J.; Botton, G.A. Formation of the ternary complex hydride Mg_2FeH_6 from magnesium hydride (β-MgH_2) and Iron: An electron microscopy and energy-loss spectroscopy study. *J. Phys. Chem. C* **2012**, *116*, 25701–25714.
29. Larson, A.C.; von Dreele, R.B. *General Structure Analysis System (GSAS)*; Los Alamos National Laboratory: Los Alamos, NM, USA, 2004; Volume 748, p. 224.
30. Toby, B.H. EXPGUI, a graphical user interface for GSAS. *J. Appl. Crystallogr.* **2001**, *34*, 210–213.
31. Vincent, S.D.; Huot, J. Effect of air contamination on ball milling and cold rolling of magnesium hydride. *J. Alloys Compd.* **2011**, *509*, L175–L179.

© 2014 by the authors; licensee MDPI, Basel, Switzerland. This article is an open access article distributed under the terms and conditions of the Creative Commons Attribution license (http://creativecommons.org/licenses/by/3.0/).